

Strong gravitational lensing in a black-hole spacetime dominated by dark energyChikun Ding,^{*} Changqing Liu, Yuanyuan Xiao, and Liqun Jiang*Department of Physics and Information Engineering, Hunan University of Humanities, Science and Technology, Loudi, Hunan 417000, Peoples Republic of China*Rong-Gen Cai[†]*State Key Laboratory of Theoretical Physics, Institute of Theoretical Physics, Chinese Academy of Sciences, Beijing 100190, Peoples Republic of China*

(Received 24 August 2013; published 12 November 2013; publisher error corrected 19 November 2013)

We study the influence of phantom fields on strong field gravitational lensing. Supposing that the gravitational field of the supermassive central object of the Galaxy is described by a phantom black hole metric, we estimate the numerical values of the coefficients and observations and find that the influence of the phantom fields is somewhat similar to that of the electric charge in a Reissner-Nordström black hole, i.e., the deflect angle and angular separation increase with the phantom constant b . However, other observations are contrary to the Reissner-Nordström case and show the effects of dark energy, such as (i) compressing the usual black hole and more powerfully attracting photons, (ii) making the relativistic Einstein ring larger than that of the usual black hole, and (iii) not weakening the usual relative magnitudes, which will facilitate observations.

DOI: [10.1103/PhysRevD.88.104007](https://doi.org/10.1103/PhysRevD.88.104007)

PACS numbers: 04.70.-s, 95.30.Sf, 95.36.+x, 97.60.Lf

I. INTRODUCTION

Modern observational programs—including type Ia supernovae, cosmic microwave background anisotropy, and mass power spectrum observations [1]—indicate that the Universe is expanding with an acceleration that is dominated to about 70% by a peculiar kind of matter called dark energy (characterized by negative values of the pressure-to-density ratio ω), while the remaining 30% consists of baryonic and nonbaryonic visible and dark matter. The simplest way to describe this dark energy is through the use of quintessence ($-1 < \omega < -1/3$) or a phantom scalar field ($\omega \leq -1$) instead of a canonical one, that is, a scalar with a negative sign for the kinetic term in the Lagrangian [2]. The values $\omega < -1$ should be noted because they seem to be not only admissible but even preferable for describing an increasing acceleration, which follows from the most recent estimates: $\omega = -1.10 \pm 0.14(1\sigma)$ [3] (according to the 7-year WMAP data) and $\omega = -1.069^{+0.091}_{-0.092}$ [4] (mainly from data on type Ia supernovae from the SNLS3 sample). Thus, $\omega = -1$ is commonly admitted by observations as a possible dark energy model. Through this connection, cosmological models with phantom scalar fields have gained considerable attention in recent years [5].

If such a phantom scalar is part of the real field content of our Universe, it is natural to seek its manifestations not only in cosmology but in local phenomena as well, in particular in black hole physics, such as dark energy accretion onto black holes [6], black hole interactions with a phantom

shell [7], the existence of regular black holes from a system of gravity coupled to these phantom fields [8], etc. How do we test these phantom fields? The best approach would be gravitational lensing, as its resolution ratio is many orders of magnitude higher than any artificial telescope [9]. Gravitational lenses are now used to determine the Hubble constant [10], probe the structure of galaxies [11], measure the density of cosmic strings [12], and restrict the density factor of the Universe [11]. Microlensing—such as that arising from stars and black holes—is used to probe dark matter and dark energy in the Galactic halo [13], etc., so we can use it here to probe the existence and distribution of dark energy via the influence of a phantom scalar on the gravitational field, i.e., on a black hole lens' behavior.

The earlier studies of gravitational lensing were developed in the weak-field approximation [14–16]. It is enough for us to investigate the properties of gravitational lensing by ordinary stars and galaxies. However, when the lens is a black hole, a strong-field treatment of gravitational lensing [17–22] is needed instead. Virbhadra and Ellis [19] found that near the line connecting the source and the lens, an observer would detect two infinite sets of faint relativistic images on each side of the black hole. These relativistic images could provide a profound verification of alternative theories of gravity. Thus, the study of strong gravitational lensing has become appealing in recent years. On the basis of the Virbhadra-Ellis lens equation [20,21], Bozza [23] extended the analytical method of lensing for a general class of static and spherically symmetric spacetimes and showed that the logarithmic divergence of the deflection angle at the photon sphere is a common feature. Bhadra *et al.* [24,25] considered Gibbons-Maeda-Garfinkle-Horowitz-Strominger black hole lensing. Eiroa *et al.* [26]

^{*}dingchikun@163.com[†]cairg@itp.ac.cn

studied Reissner-Nordström black hole lensing. Konoplya [27] studied the corrections to the deflection angle and time delay of black hole lensing immersed in a uniform magnetic field. Majumdar [28] investigated dilaton–de Sitter black hole lensing. Perlick [29] obtained an exact lens equation and used it to study Barriola-Vilenkin monopole black hole lensing. Virbhadra *et al.* studied the relativistic images of spherically symmetric black hole lensing without any approximations (i.e., the strong- or weak-field treatments) [30]. S. Chen studied Kehagias-Sfetsos black hole lensing [31]. Bin-Nun [32] studied the strong gravitational lensing by Sgr A*, G.N. Gylchev studied phantom black hole lensing [33], and so on.

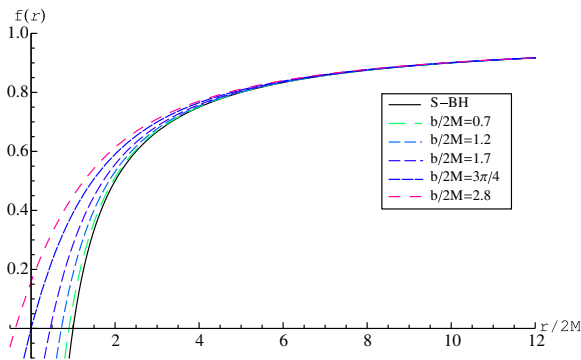
This paper is organized as follows. In Sec. II we briefly review the regular phantom black holes. In Sec. III we adopt Bozza’s method and obtain the deflection angles for light rays propagating in the phantom black hole space-time. In Sec. IV we discuss the time delay of light seen from images. In Sec. V we suppose that the gravitational field of the supermassive black hole at the center of our Galaxy can be described by this metric and then obtain the numerical results for the observational gravitational lensing parameters defined in Secs. III and IV. Then, we make a comparison between the properties of gravitational lensing in the phantom black hole and Reissner-Nordström metrics. In Sec. VI we present a summary.

II. PHANTOM BLACK HOLES

Consider the Lagrangian

$$L = \sqrt{-g} \left[-\frac{R}{8\pi G} + \epsilon g^{\alpha\beta} \phi_{;\alpha} \phi_{;\beta} - 2V(\phi) \right], \quad (2.1)$$

which includes a scalar field, in general, with some potential $V(\phi)$; ϵ distinguishes normal, canonical scalar fields ($\epsilon = +1$) and phantom fields ($\epsilon = -1$). The static, spherically symmetric metric for phantom scalar fields can be written in the form [8]



$$ds^2 = -f(r)dt^2 + \frac{dr^2}{f(r)} + (r^2 + b^2)(d\theta^2 + \sin^2\theta d\phi^2), \quad (2.2)$$

with

$$f(r) = 1 - \frac{3M}{b} \left[\left(\frac{\pi}{2} - \arctan \frac{r}{b} \right) \left(1 + \frac{r^2}{b^2} \right) - \frac{r}{b} \right], \quad (2.3)$$

where M is the black hole’s mass defined in the usual way, b is a positive constant relative to the charge of phantom scalar fields (termed the phantom constant), and its potential is

$$\frac{\phi}{\sqrt{2}} \equiv \psi = \arctan \frac{r}{b},$$

$$V = \frac{3M}{b^3} \left[\left(\frac{\pi}{2} - \psi \right) (3 - 2\cos^2\psi) - 3\sin\psi \cos\psi \right]. \quad (2.4)$$

This metric behavior is controlled by two integration constants: b and M . When $M = 0$, this is an Ellis wormhole. If $M < 0$, it is a wormhole which is asymptotically flat at $r \rightarrow \infty$ and which has an anti–de Sitter metric at $r \rightarrow -\infty$. When $M > 0$, it is a regular black hole whose curvature scalar at the origin is

$$R_{\mu\nu\tau\rho} R^{\mu\nu\tau\rho} = \frac{3(4b^2 - 8bM\pi + 9\pi^2 M^2)}{b^6}, \quad (2.5)$$

and it has a Schwarzschild-like causal structure at large r . In Fig. 1 we show the behavior of the black holes’ metric functions (2.3) and the energy density and pressure for the phantom field. In Table I its horizon, pressure, and pressure-to-density ratio at the horizon for different values of b are listed.

From Table I we can see that if the phantom constant is small or even if $b \rightarrow 0$, then the black hole behaves as a Schwarzschild black hole [it cannot recover a Schwarzschild black hole due to the fact that $b \neq 0$ from Eq. (2.5)]. In this case we can call it a phantom

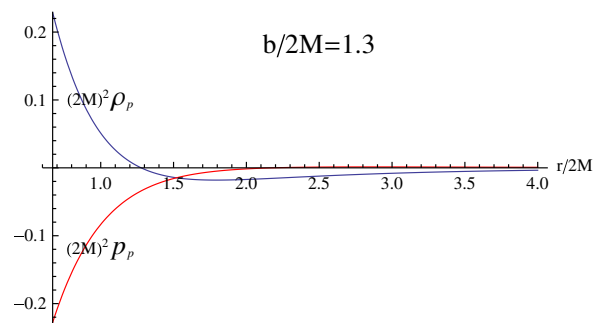


FIG. 1 (color online). Left: The metric functions of the regular phantom black hole for different values of b . The solid line is described by the expression $f(r) = 1 - 2M/r$ for a Schwarzschild black hole, “S-BH.” Right: The energy density ρ_p and pressure p_p for a phantom field with $b/2M = 1.3$.

TABLE I. Numerical values for the radius of the single event horizon of a phantom black hole, the pressure-to-density ratio ω_p , and the pressure p_+ for phantom fields near the horizon for different values of the phantom constant b . Here, $\omega_p = -1 + \omega \times 10^{-7}$.

$b/2M$	0.02	0.1	0.4	0.7	1.0	1.3	1.6	1.9	2.2	2.3	$3\pi/4$
$r_+/2M$	0.99992	0.998001	0.968143	0.90329	0.805076	0.675537	0.51679	0.330846	0.119525	0.043730	0
ω	3.2612	-7.1203	4.0101	3.4691	1.02028	-1.71816	1.05262	0.996388	1.17354	-0.03441	0.0
$-(2M)^2 p_+$	0.000160	0.003966	0.056039	0.133647	0.194823	0.224111	0.226573	0.212936	0.191999	0.184419	0.180127

Schwarzschild black hole. When b increases, the radius of the horizon decreases and $-p_+$ increases, which indicates a stronger effect from dark energy. The pressure-to-energy-density ratio ω_p of this dark energy is around -1 , which is coincident with present observations [3,4]. The expressions for ω_p , ρ_p , and p_p are included in the Appendix. Table I also shows that phantom fields affect the size of the black hole. In addition, the phantom constant b behaves somewhat like the electric charge q in a Reissner-Nordström black hole (whose external horizon decreases with q), so we can compare phantom black hole lensing to Reissner-Nordström lensing. The line element (2.2) describes the geometry of a phantom black hole and should give us useful insights about possible dark energy effects on strong gravitational lensing.

III. DEFLECTION ANGLE IN THE PHANTOM BLACK HOLE SPACETIME

From this section and hereafter, we set $b/2M = b$, $r_+/2M = r$, $u/2M = u$, and $q/2M = q$, and rewrite the metric (2.2) as

$$ds^2 = -A(r)dt^2 + B(r)dr^2 + C(r)(d\theta^2 + \sin^2\theta d\phi^2), \tag{3.1}$$

with

$$A(r) = f(r), \quad B(r) = 1/f(r), \quad C(r) = r^2 + b^2. \tag{3.2}$$

The deflection angle for the photon coming from infinity can be expressed as

$$\alpha(r_0) = I(r_0) - \pi, \tag{3.3}$$

where r_0 is the closest approach distance and $I(r_0)$ is [20,21]

$$I(r_0) = 2 \int_{r_0}^{\infty} \frac{\sqrt{B(r)}dr}{\sqrt{C(r)}\sqrt{\frac{C(r)A(r_0)}{C(r_0)A(r)} - 1}}. \tag{3.4}$$

It is easy to see that as the parameter r_0 decreases the deflection angle increases. At a certain point, the deflection angle will become 2π , which means that the light ray will make a complete loop around the compact object before reaching the observer. When r_0 is equal to the radius of the photon sphere, the deflection angle diverges and the photon is captured.

The photon-sphere equation is given by [20,21]

$$\frac{C'(r)}{C(r)} = \frac{A'(r)}{A(r)}, \tag{3.5}$$

which admits at least one positive solution, and then the largest real root of Eq. (3.5) is defined as the radius of the photon sphere. Using the phantom black hole metric (2.2), Eq. (3.5) is

$$\frac{2r}{r^2 + b^2} = \frac{\frac{3}{b^2}[1 - (\frac{\pi}{2} - \arctan \frac{r}{b})\frac{r}{b}]}{1 - \frac{3}{2b}[(\frac{\pi}{2} - \arctan \frac{r}{b})(1 + \frac{r^2}{b^2}) - \frac{r}{b}]}. \tag{3.6}$$

After a simple calculation, this can be simplified to $2r = 3$, so that the radius of the photon sphere can be given by

$$r_{ps} = \frac{3}{2}, \tag{3.7}$$

which is the same as that of a Schwarzschild black hole and is independent of the constant b . It tells us that (i) no matter how the phantom fields are distributed the photon sphere stays the same, and (ii) we cannot distinguish merely from the photon sphere whether dark energy exists or not.

Following the method developed by Bozza¹ [23,31], we define a variable

$$z = 1 - \frac{r_0}{r}, \tag{3.8}$$

and obtain

$$I(r_0) = \int_0^1 R(z, r_0)f(z, r_0)dz, \tag{3.9}$$

where

$$R(z, r_0) = \frac{2r_0\sqrt{A(r)B(r)C(r_0)}}{C(r)(1-z)^2} = \frac{2r_0\sqrt{r_0^2 + b^2}}{(r^2 + b^2)(1-z)^2}, \tag{3.10}$$

$$f(z, r_0) = \frac{1}{\sqrt{A(r_0) - A(r)C(r_0)/C(r)}}. \tag{3.11}$$

The function $R(z, r_0)$ is regular for all values of z and r_0 . However, $f(z, r_0)$ diverges as z tends to zero. Thus, we split the integral (3.9) into two parts,

¹Though Bozza's prescriptions have been subjected to much criticism of inaccuracy [30], it can give us a clear picture of strong gravitational lensing from an analytic point of view. For numerical works without any approximations on spherically symmetric black hole lensing please see Ref. [30].

$$I_D(r_0) = \int_0^1 R(0, r_{\text{ps}}) f_0(z, r_0) dz, \quad (3.12)$$

$$I_R(r_0) = \int_0^1 [R(z, r_0) f(z, r_0) - R(0, r_{\text{ps}}) f_0(z, r_0)] dz,$$

where $I_D(r_0)$ and $I_R(r_0)$ denote the divergent and regular parts in the integral (3.9), respectively. To find the order of divergence of the integrand, we expand the argument of the square root in $f(z, r_0)$ to the second order in z and obtain the function $f_0(z, r_0)$:

$$f_0(z, r_0) = \frac{1}{\sqrt{p(r_0)z + q(r_0)z^2}}, \quad (3.13)$$

where

$$p(r_0) = \frac{r_0(2r_0 - 3)}{r_0^2 + b^2}, \quad (3.14)$$

$$q(r_0) = \frac{r_0^2}{r_0^2 + b^2} + \frac{r_0(2r_0 - 3)(b^2 - r_0^2)}{(r_0^2 + b^2)^2}.$$

When r_0 is equal to the radius of the photon sphere r_{ps} , the coefficient $p(r_0)$ vanishes, and the leading term of the divergence in $f_0(z, r_0)$ is z^{-1} ; thus, the integral (3.9) diverges logarithmically. Close to the divergence, Bozza [23] found that the deflection angle can be expanded in the form

$$\alpha(\theta) = -\bar{a} \log\left(\frac{\theta D_{\text{OL}}}{u_{\text{ps}}} - 1\right) + \bar{b} + O(u - u_{\text{ps}}), \quad (3.15)$$

where

$$\begin{aligned} \bar{a} &= 1, \\ \bar{b} &= -\pi + b_R + \bar{a} \log \frac{4q^2(r_{\text{ps}})[2A(r_{\text{ps}}) - (r_{\text{ps}}^2 + b^2)A''(r_{\text{ps}})]}{p'^2(r_{\text{ps}})u_{\text{ps}}\sqrt{A^3(r_{\text{ps}})(r_{\text{ps}}^2 + b^2)}}, \\ b_R &= I_R(r_{\text{ps}}), \quad p'(r_{\text{ps}}) = \left. \frac{dp}{dr_0} \right|_{r_0=r_{\text{ps}}}, \\ u_{\text{ps}} &= \frac{\sqrt{r_{\text{ps}}^2 + b^2}}{\sqrt{A(r_{\text{ps}})}}. \end{aligned} \quad (3.16)$$

D_{OL} denotes the distance between the observer and the gravitational lens, and \bar{a} and \bar{b} are the so-called strong-field-limit coefficients which depend on the metric functions evaluated at r_{ps} . In general, the coefficient b_R cannot be calculated analytically, but in this case it can be evaluated numerically.

We can now obtain \bar{b} and u_{ps} , which we show in Fig. 2. Figure 2 shows us that as b increases the coefficient \bar{b} always decreases, whereas in the Reissner-Nordström case there is a region of increase with the electric charge q .

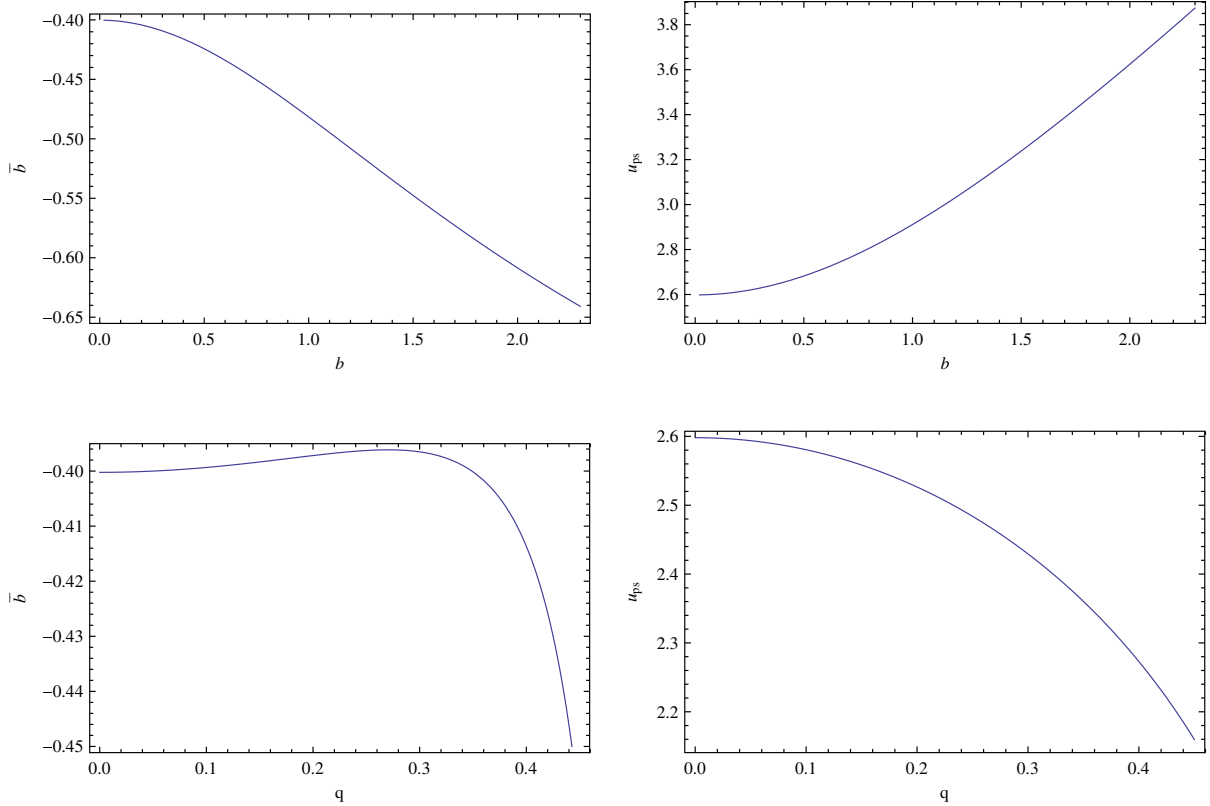


FIG. 2 (color online). The coefficient of the strong-field limit \bar{b} and the minimum impact parameter u_{ps} vs the phantom constant b in the phantom black hole spacetime (upper panels) and vs q in the Reissner-Nordström black hole spacetime (lower panels). The values of the coefficient of Reissner-Nordström lensing come from Ref. [23].

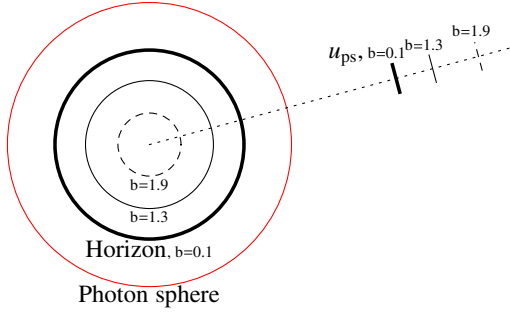


FIG. 3 (color online). The position of the photon sphere, black hole horizon, and minimum impact parameter u_{ps} for different values of the phantom constant b .

Also, the minimum impact parameter u_{ps} increases, which is contrary to the case in the Reissner-Nordström black hole spacetime. This behavior will greatly affect both the deflect angle and the angular separation. Figure 3 shows the relative position of the photon sphere, the black hole horizon, and the minimum impact parameter for different values of b . A larger u_{ps} indicates that at greater distances the deflect angle of the photons will also diverge. It is easy to see that a larger phantom constant corresponds to a stronger interaction of dark energy on the spacetime, which causes it to curve, i.e., compresses the black hole and more powerfully attracts photons. In principle we can distinguish a phantom black hole from the Reissner-Nordström black hole and probe the value of the phantom constant by using strong field gravitational lensing.

Figure 4 shows the deflection angle $\alpha(\theta)$ evaluated at $u = u_{ps} + 0.00326$. It indicates that the presence of b increases the deflection angle $\alpha(\theta)$ for the light propagated in the phantom black hole spacetime, which is similar to the electric charge q in the Reissner-Nordström case. Comparing with the Reissner-Nordström case, we could extract the information about the size of the phantom constant b by using strong field gravitational lensing.

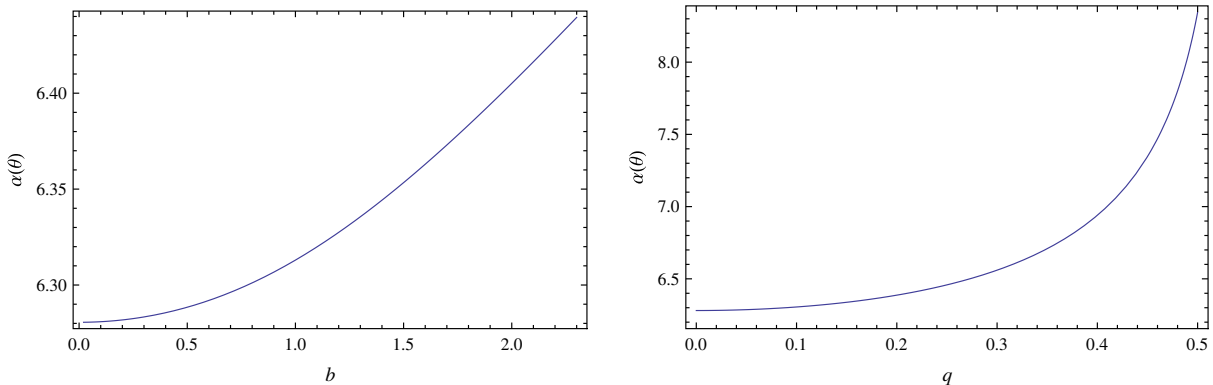


FIG. 4 (color online). Deflection angles in the phantom black hole (left) and Reissner-Nordström (right) spacetimes evaluated at $u = u_{ps} + 0.00326$.

Assuming that the source, lens, and observer are highly aligned, the lens equation in strong gravitational lensing can be written as [34]

$$\tan \beta = \tan \theta - \frac{D_{LS}}{D_{OS}} [\tan \theta + \tan (\Delta \alpha_n - \theta)], \quad (3.17)$$

where D_{LS} is the distance between the lens and the source, $D_{OS} = D_{LS} + D_{OL}$, β is the angular separation between the source and the lens, θ is the angular separation between the image and the lens, and $\Delta \alpha_n = \alpha - 2n\pi$ is the offset of deflection angle with n an integer. The position of the n th relativistic image can be approximated as

$$\theta_n = \theta_n^0 + \frac{u_{ps} e_n (\beta - \theta_n^0) D_{OS}}{\bar{a} D_{LS} D_{OL}}, \quad (3.18)$$

where

$$e_n = e^{\frac{i-2n\pi}{a}}. \quad (3.19)$$

θ_n^0 are the image positions corresponding to $\alpha = 2n\pi$. The magnification of the n th relativistic image is given by

$$\mu_n = \frac{u_{ps}^2 e_n (1 + e_n) D_{OS}}{\bar{a} \beta D_{LS} D_{OL}^2}. \quad (3.20)$$

If θ_∞ represents the asymptotic position of a set of images in the limit $n \rightarrow \infty$, the minimum impact parameter u_{ps} can be simply obtained as

$$u_{ps} = D_{OL} \theta_\infty. \quad (3.21)$$

In the simplest situation, we consider only that the outermost image θ_1 is resolved as a single image and all the remaining ones are packed together at θ_∞ . Then the angular separation between the first image and the other ones can be expressed as

$$s = \theta_1 - \theta_\infty, \quad (3.22)$$

and the ratio of the flux from the first image and that from the all other images is given by

$$\mathcal{R} = \frac{\mu_1}{\sum_{n=2}^{\infty} \mu_n}. \quad (3.23)$$

For a highly aligned source, lens, and observer geometry, these observables can be simplified as

$$s = \theta_{\infty} e^{\frac{\bar{b}-2\pi}{\bar{a}}}, \quad \mathcal{R} = e^{\frac{2\pi}{\bar{a}}}. \quad (3.24)$$

The strong deflection limit coefficients \bar{a} , \bar{b} and the minimum impact parameter u_{ps} can be obtained by measuring s , \mathcal{R} and θ_{∞} . Then, comparing their values with those predicted by the theoretical models, we can identify the nature of the black hole lens.

IV. TIME DELAY IN THE PHANTOM BLACK HOLE SPACETIME

In this section we consider the time delay of light seen from images. Weinberg [35] obtained the time required for light to travel from a source at coordinates $(r, \theta = \pi/2, \varphi = \varphi_1)$ to the closest point of approach (to the lens) at coordinates $(r_0, \theta = \pi/2, \varphi = \varphi_2)$ by solving null geodesic equations for a general static spherically symmetric spacetime. A straightforward calculation for the metric (2.2) gives the time delay as [30]

$$\begin{aligned} \tau(r_0) &= 2M \left[\int_{r_0}^{\chi_s} \frac{dr}{F(r)} + \int_{r_0}^{\chi_o} \frac{dr}{F(r)} \right] - D_{\text{OS}} \sec \beta, \\ F(r) &= f(r) \sqrt{1 - \frac{f(r)(r_0^2 + b^2)}{f(r_0)(r^2 + b^2)}}, \end{aligned} \quad (4.1)$$

with

$$\chi_s = \frac{D_{\text{OS}}}{2M} \sqrt{(D_{\text{LS}}/D_{\text{OS}})^2 + \tan^2 \beta}, \quad \chi_o = \frac{D_{\text{OL}}}{2M}. \quad (4.2)$$

In the next section we will use Eqs. (3.18), (3.17), and (4.1) to obtain the numerical values for the offset of the deflection angle $\Delta\alpha_{1p}$ and the time delay τ_{1p} of the first relativistic images (on the same side as the primary image).

V. NUMERICAL ESTIMATION OF OBSERVATIONAL GRAVITATIONAL LENSING PARAMETERS

In this section—supposing that the gravitational field of the supermassive black hole at the Galactic Center of the Milky Way can be described by the phantom black hole metric—we estimate the numerical values for the coefficients and observables of strong gravitational lensing, and then we study the effect of the phantom constant b on the gravitational lensing.

The mass of the central object of our Galaxy is estimated to be $2.8 \times 10^6 M_{\odot}$ and its distance is around 8.5 kpc [36]. For different values of b , the numerical values of the minimum impact parameter u_{ps} , the angular position of the asymptotic relativistic images θ_{∞} , the angular separation s , and the relative magnification of the outermost relativistic image with the other relativistic images r_m are listed in Table II.

It is easy to obtain that our results reduce to those in the Schwarzschild black hole spacetime as $b \rightarrow 0$. Moreover, from Table II we also find that as the parameter b increases, the minimum impact parameter u_{ps} and the angular position of the relativistic images θ_{∞} increase as well, which is contrary to the Reissner-Nordström case. The appearance of θ_{∞} tells us that the relativistic Einstein ring is much bigger than the Schwarzschild lensing. The angular separation s appears to behave similarly as in the Reissner-Nordström case. Also, the relative magnitude r_m stays the same as in Schwarzschild lensing, that is to say, the relative flux of the first image is not affected by phantom scalar fields (dark energy).

From Fig. 5 we can see that for the phantom black hole an increase of the parameter b causes an increase of both the angular position θ_{∞} and the angular separation s . This means that the bending angle is bigger in the phantom black hole spacetime. In order to identify the nature of the lensing of these two compact objects, it is necessary to measure the angular separation s and the relative magnification r_m in the astronomical observations. Table II tells us that the resolution of the extreme angular separation image is $\sim 0.025 \mu$ arcsecond, which is too small. However, as new technologies are developed the effects of the phantom

TABLE II. Numerical estimations for the main observables and the strong-field limit coefficients for a black hole at the center of our Galaxy, which is assumed to be described by the phantom black hole metric. R_s is the Schwarzschild radius and $r_m = 2.5 \log \mathcal{R}$.

	Phantom black hole						Reissner-Nordström black hole			
	$b = 0.02$	$b = 0.1$	$b = 0.7$	$b = 1.3$	$b = 1.9$	$b = 2.3$	$q = 0.1$	$q = 0.2$	$q = 0.3$	$q = 0.4$
θ_{∞} (μ arg sec)	16.8708	16.8923	17.9149	20.1181	23.009	25.1555	16.7565	16.405	15.7743	14.759
s (μ arg sec)	0.021112	0.021119	0.021445	0.022306	0.023651	0.024749	0.021635	0.0234359	0.027538	0.037984
r_m	6.82188	6.82188	6.82188	6.82188	6.82188	6.82188	6.79094	6.68985	6.48575	6.07378
u_m/R_s	2.59821	2.60154	2.75902	3.09832	3.54355	3.87412	2.58062	2.52649	2.42935	2.27299
\bar{a}	1	1	1	1	1	1	1.00456	1.01974	1.05183	1.12317
\bar{b}	-0.40027	-0.40125	-0.44471	-0.52133	-0.59706	-0.64085	-0.39935	-0.39718	-0.39651	-0.41364

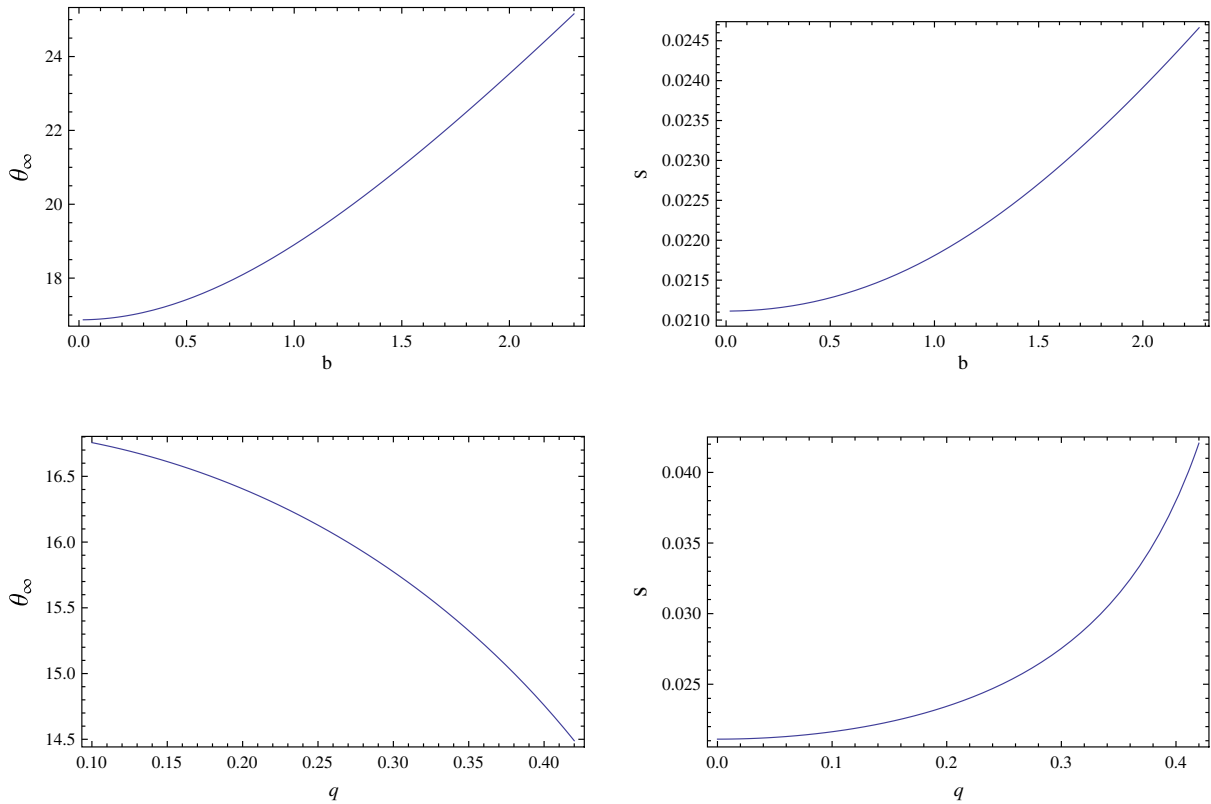


FIG. 5 (color online). Strong gravitational lensing by the Galactic Center black hole. We plot the values of the angular position θ_∞ , the relative magnitudes r_m , and the angular separation s vs the phantom constant b in the phantom black hole spacetime (upper panels) and vs q in the Reissner-Nordström black hole (lower panels).

constant b on gravitational lensing may be detected in the future.

Observations of the time delay are given in Table III. By comparing the results with those in Ref. [30], we can see that both the relativistic Einstein ring (when $\beta = 0$) and the time delay become larger with the phantom constant b .

VI. SUMMARY

Modern observations show that the Universe is expanding with an acceleration that is dominated by a peculiar kind of matter (e.g., dark energy) which can be modeled by quintessence or phantom scalar fields. This unknown matter has unusual properties such as negative values of the pressure-to-density ratio. If it exists, then it will inevitably

TABLE III. Numerical values for the offset of the deflection angle $\Delta\alpha_{1p}$ and time delay τ_{1p} of the first relativistic images (on the same side as the primary image) with different values for a constant b and angular source position β . Here β , $\Delta\alpha_{1p}$, and τ_{1p} are, respectively, expressed in arcseconds (arcsec), microarcseconds (μas), and minutes (min). In order to compare the results with those in Ref. [30], we here apply the most recent data for our Galaxy [37]. We suppose that the mass $M = 3.61 \times 10^6 M_\odot$ and the distance $D_{\text{OL}} = 7.62$ kpc, so that $M/D_{\text{OL}} \approx 2.26 \times 10^{-11}$ and $D_{\text{OL}}/D_{\text{OS}} = 1/2$.

β (arcsec)	$b = 0.02$		$b = 0.5$		$b = 1.0$		$b = 2.0$		$b = 3\pi/4$	
	$\Delta\alpha_{1p}$ (μas)	τ_{1p} (min)								
0	48.60849	38.3701	50.17959	38.4742	54.45789	39.3316	67.78770	42.3771	73.35538	43.5699
10^{-6}	46.60849	38.3702	48.17959	38.4742	52.45789	39.3316	65.78770	42.3771	71.35538	43.5699
10^{-5}	28.60848	38.3703	30.17959	38.4742	34.45789	39.3316	47.78770	42.3771	53.35538	43.5699
10^{-4}	-151.392	38.3704	-149.820	38.4742	-145.542	39.3316	-132.212	42.3771	-126.645	43.5699
10^{-3}	-1951.39	38.3706	-1949.82	38.4742	-1945.54	39.5665	-1932.21	42.3771	-1926.64	43.5699
10^{-2}	-19951.4	38.3708	-19949.8	38.4742	-19945.5	39.5695	-19932.2	42.3772	-19926.6	43.5699
10^{-1}	-199951	38.3732	-199949	38.4772	-199945	39.5752	-199932	42.3802	-199926	43.5730
1	-1999951	38.4752	-1999949	38.7812	-1999945	39.8736	-1999932	42.6841	-1999926	43.8769

affect known spacetimes such as black hole physics. Studying strong gravitational lensing can help us probe its existence and properties from astronomical observations. We have investigated strong-field lensing in the phantom black hole spacetime to study the influence of the phantom constant on strong gravitational lensing. The model was applied to the supermassive black hole at the Galactic Center.

Our results show that with an increase of the phantom constant b both the minimum impact parameter u_{ps} and the angular position of the relativistic images θ_∞ increase, which is contrary to the case of Reissner-Nordström black hole lensing with an electric charge q . The photon sphere r_{ps} and relative magnitudes r_m stay the same as those of a Schwarzschild black hole and are independent of b , which is also contrary to the case where they are weakened by an electric charge. However, the deflect angle $\alpha(\theta)$ and the angular separation s appear to have similar behavior as in Reissner-Nordström lensing. This may offer a way to distinguish a phantom black hole from a Reissner-Nordström one using the astronomical instruments developed in the future.

Our results also show the effects of dark energy in the considered model, such as (i) compressing the usual black hole and more powerfully attracting photons, (ii) making the relativistic Einstein ring larger than the usual black hole, and (iii) not weakening the usual relative magnitudes, which will facilitate observations.

Two days after this paper was published to the arXiv, Ref. [38] appeared online in the same database, containing a partial overlap with our work.

ACKNOWLEDGMENTS

This work was supported by the National Natural Science Foundation of China under No. 11247013, the Hunan Provincial NSFC No. 11JJ3014, the Scientific Research Fund of the Hunan Provincial Education Department No. 11B067, the Foundation for the Author of Hunan Provincial Excellent Doctoral Dissertation No. YB2012B034, and the Aid program for the Science and Technology Innovative Research Team in Higher Educational Institutions of Hunan Province.

APPENDIX: ENERGY DENSITY AND PRESSURE OF PHANTOM FIELDS

With the metric (2.2), the components for the energy-momentum tensor of phantom fields are

$$\begin{aligned} T_0^0 &= -\frac{rf'}{b^2+r^2} - \frac{(2b^2+r^2)f}{(b^2+r^2)^2} + \frac{1}{b^2+r^2}, \\ T_1^1 &= -\frac{rf'}{b^2+r^2} - \frac{r^2f}{(b^2+r^2)^2} + \frac{1}{b^2+r^2}, \\ T_2^2 = T_3^3 &= -\frac{rf'}{b^2+r^2} - \frac{b^2f}{(b^2+r^2)^2} - \frac{f''}{2}. \end{aligned} \quad (\text{A1})$$

We can rewrite them as an appropriate general expression [39],

$$\begin{aligned} T_0^0 &= \rho_p(r), \\ T_i^j &= C(r)r_i r^j + B(r)\delta_i^j \\ &= 3\rho_p(r)\omega_p \left[-(1+3D)\frac{r_i r^j}{r_n r^n} + D\delta_i^j \right], \end{aligned} \quad (\text{A2})$$

so that the spatial part is proportional to the time component with the arbitrary parameter D depending on the internal structure of the phantom fields. An isotropic averaging over the angles gives

$$\langle T_i^j \rangle = -\rho_p(r)\omega_p \delta_i^j = -p_p(r)\delta_i^j, \quad (\text{A3})$$

and therefore $p_p(r) = \omega_p \rho_p(r)$. After such a treatment, the results are

$$\begin{aligned} T_1^1 &= \rho_p(r) + \frac{2b^2f}{(b^2+r^2)^2}, \\ T_2^2 = T_3^3 &= -\frac{1}{2}(3\omega_p + 1)\rho_p(r) - \frac{b^2f}{(b^2+r^2)^2}. \end{aligned} \quad (\text{A4})$$

At last, we obtain the expressions for the pressure and pressure-to-energy density ratio,

$$\begin{aligned} \omega_p &= \frac{(2b^2+r^2)f + (b^2+r^2)[(b^2+r^2)f'' + 3rf' - 1]}{3[(2b^2+r^2)f + (b^2+r^2)(rf' - 1)]}, \\ p_p(r) &= \frac{rf'}{b^2+r^2} + \frac{f''}{3} + \frac{(2b^2+r^2)f}{3(b^2+r^2)^2} - \frac{1}{3(b^2+r^2)}. \end{aligned} \quad (\text{A5})$$

-
- [1] N. A. Bachall, J. P. Ostriker, S. Perlmutter, and P. J. Steinhardt, *Science* **284**, 1481 (1999); S. J. Perlmutter *et al.*, *Astrophys. J.* **517**, 565 (1999); V. Sahni and A. A. Starobinsky, *Int. J. Mod. Phys. D* **09**, 373 (2000).
[2] K. A. Bronnikov, R. A. Konoplya, and A. Zhidenko, *Phys. Rev. D* **86**, 024028 (2012).
[3] E. Komatsu, *Astrophys. J. Suppl. Ser.* **192**, 18 (2011).
[4] M. Sullivan *et al.*, *Astrophys. J.* **737**, 102 (2011).
[5] R. Gannouji, D. Polarski, A. Ranquet, and A. A. Starobinsky, *J. Cosmol. Astropart. Phys.* **09** (2006) 016; A. Vikman, *Phys. Rev. D* **71**, 023515 (2005); R. R. Caldwell, M. Kamionkowski, and N. N. Weinberg, *Phys. Rev. Lett.* **91**, 071301 (2003); S. Chattopadhyay and U. Debnath, *Braz. J. Phys.* **39**, 86 (2009); Z. Y. Sun and Y. G. Shen, *Gen. Relativ. Gravit.* **37**, 243 (2005); L. P. Chimento and R. Lazkoz, *Phys. Rev. Lett.* **91**, 211301 (2003).

- [6] E. O. Babichev, V. I. Dokuchaev, and Yu. N. Eroshenko, *Phys. Rev. Lett.* **93**, 021102 (2004); A. V. Frolov, *Phys. Rev. D* **70**, 061501 (2004).
- [7] V. Berezin, V. Dokuchaev, Y. Eroshenko, and A. Smirnov, *Classical Quantum Gravity* **22**, 4443 (2005).
- [8] K. A. Bronnikov and J. C. Fabris, *Phys. Rev. Lett.* **96**, 251101 (2006).
- [9] B. McBreen and L. Metcalfe, *Nature (London)* **330**, 348 (1987).
- [10] C. C. Dyer and R. C. Roeder, *Astrophys. J.* **241**, L133 (1980).
- [11] X. P. Wu, *Astron. Astrophys.* **214**, 43 (1989).
- [12] J. R. Gott, *Nature (London)* **321**, 420 (1986).
- [13] K. Chang and S. Refsdal, *Nature (London)* **282**, 561 (1979).
- [14] P. Schneider, J. Ehlers, and E. E. Falco, *Gravitational Lenses* (Springer-Verlag, Berlin, 1992).
- [15] A. F. Zakharov, *Gravitational Lenses and Microlenses* (Janus-K, Moscow, 1997).
- [16] R. D. Blandford and R. Narayan, *Annu. Rev. Astron. Astrophys.* **30**, 311 (1992).
- [17] C. Darwin, *Proc. R. Soc. London* **249**, 180 (1959).
- [18] K. S. Virbhadra, D. Narasimha, and S. M. Chitre, *Astron. Astrophys.* **337**, 1 (1998).
- [19] K. S. Virbhadra and G. F. R. Ellis, *Phys. Rev. D* **62**, 084003 (2000).
- [20] C. M. Claudel, K. S. Virbhadra, and G. F. R. Ellis, *J. Math. Phys. (N.Y.)* **42**, 818 (2001).
- [21] K. S. Virbhadra and G. F. R. Ellis, *Phys. Rev. D* **65**, 103004 (2002).
- [22] S. Frittelli, T. P. Kling, and E. T. Newman, *Phys. Rev. D* **61**, 064021 (2000).
- [23] V. Bozza, *Phys. Rev. D* **66**, 103001 (2002).
- [24] A. Bhadra, *Phys. Rev. D* **67**, 103009 (2003).
- [25] K. Sarkar and A. Bhadra, *Classical Quantum Gravity* **23**, 6101 (2006).
- [26] E. F. Eiroa, G. E. Romero, and D. F. Torres, *Phys. Rev. D* **66**, 024010 (2002).
- [27] R. A. Konoplya, *Phys. Rev. D* **74**, 124015 (2006); *Phys. Lett. B* **644**, 219 (2007).
- [28] N. Mukherjee and A. S. Majumdar, *Gen. Relativ. Gravit.* **39**, 583 (2007).
- [29] V. Perlick, *Phys. Rev. D* **69**, 064017 (2004).
- [30] K. S. Virbhadra, *Phys. Rev. D* **79**, 083004 (2009); K. S. Virbhadra and C. R. Keeton, *Phys. Rev. D* **77**, 124014 (2008).
- [31] S. Chen and J. Jing, *Phys. Rev. D* **80**, 024036 (2009).
- [32] A. Y. Bin-Nun, *Classical Quantum Gravity* **28**, 114003 (2011).
- [33] G. N. Gyulchev and I. Z. Stefanov, *Phys. Rev. D* **87**, 063005 (2013).
- [34] V. Bozza, S. Capozziello, G. Lovane, and G. Scarpetta, *Gen. Relativ. Gravit.* **33**, 1535 (2001).
- [35] S. Weinberg, *Gravitation and Cosmology: Principles and Applications of the General Theory of Relativity* (Wiley, New York, 1972).
- [36] D. Richstone *et al.*, *Nature (London)* **395**, A14 (1998).
- [37] F. Eisenhauer *et al.*, *Astrophys. J.* **628**, 246 (2005).
- [38] E. F. Eiroa and C. M. Sendra, *Phys. Rev. D* **88**, 103007 (2013).
- [39] V. V. Kiselev, *Classical Quantum Gravity* **20**, 1187 (2003); S. Chen, B. Wang, and R. Su, *Phys. Rev. D* **77**, 124011 (2008).